creative commons
COMMONS DEED

저작자표시-비영리-변경금지 2.0 대한민국

이용자는 아래의 조건을 따르는 경우에 한하여 자유롭게

- 이 저작물을 복제, 배포, 전송, 전시, 공연 및 방송할 수 있습니다.

다음과 같은 조건을 따라야 합니다:

저작자표시. 귀하는 원저작자를 표시하여야 합니다.

비영리. 귀하는 이 저작물을 영리 목적으로 이용할 수 없습니다.

변경금지. 귀하는 이 저작물을 개작, 변형 또는 가공할 수 없습니다.

- 귀하는, 이 저작물의 재이용이나 배포의 경우, 이 저작물에 적용된 이용허락조건을 명확하게 나타내어야 합니다.
- 저작권자로부터 별도의 허가를 받으면 이러한 조건들은 적용되지 않습니다.

저작권법에 따른 이용자의 권리는 위의 내용에 의하여 영향을 받지 않습니다.

이것은 이용허락규약(Legal Code)을 이해하기 쉽게 요약한 것입니다.

Disclaimer

dCollection

[UCI]I804:48009-200000289916

Master of Engineering

Synthesis and Characteristics of Immiscible Fe-Cu Nanoparticles using Electrical Explosion of Wire in Liquid

University of Ulsan

Materials Science and Engineering

Chu Dac Phuc

Synthesis and Characteristics of Immiscible Fe-Cu Alloys using Electrical Explosion of Wire in Liquid

Supervisor: Prof. Jin-Chun Kim

A Dissertation

Submitted to the Graduate School of the University of Ulsan

in Partial Fulfillment of the Requirements

for the Degree of

Master of Engineering

by

Chu Dac Phuc

School of Materials Science and Engineering

University of Ulsan, Korea

Feb. 2020

This certifies that the dissertation of

Chu Dac Phuc is approved by

Committee Chairman: Prof. SANG-YONG SHIN

Committee Member: Prof. JUNG-HO JIN

Committee Member: Prof. JIN-CHUN KIM

School of Materials Science and Engineering

University of Ulsan, Korea

Feb. 2020

Chu Dac Phuc의

공학석사학위 논문을 인준함

심 사 위 원 장　　신상용 (인)

심 사 위 원　　진정호 (인)

심 사 위 원　　김진천 (인)

울산대학교 대학원

2020년 2월

Acknowledgements

I would like to express my thanks to my advisors, committee members, family, friends, colleagues and many others for their guidance, help and support. Without their help my research work would have not been finished.

First and foremost, I would like to express my deep gratitude to my advisor, Prof. Kim Jin-Chun, for his esteemed guidance, constant encouragement, and consistent support throughout my study time in the University of Ulsan. His keen insight into researching and crucial suggestions is the key factors towards the success of this work. Without his support and his guidance, this work could not be completed. His patience and trust in my abilities is what made this dissertation possible.

I am also thankful all members of Future Powder Materials and Processing Lab and all staffs at School of Materials Science and Engineering for supporting me during my time in Korea. I would like to say many thanks to the staffs in the research facilities center of University of Ulsan for helping me on the measurements of my samples.

I also would like to thank professors in the committee, Prof. Shin Sangyong, Prof. Jin Jungho and Prof. Kim Jin-Chun, for their comments and suggestions throughout this study.

I am especially grateful to my beloved family, my parents for their unconditional love and spiritual support and would like to thank them for growing me in a way to believe that I can achieve anything in my life with hard work, devotion and patience as well. Last but not the least, I would like to thank my brother and my friends who be there for me when I started a new chapter of my life in Korea.

\

Ulsan, Feb 2020

Chu Dac Phuc

Contents

List of Figures

List of Tables

Nomenclature

NPs	Nanoparticles
BNPs	Bimetallic Nanoparticles
MNPs	Monometallic Nanoparticles
PVD	Physical Vapor Deposition
EEW	Electrical Explosion of Wire
SEM	Scanning Electron Microscope
EDS	Energy-Dispersive Spectroscope
TEM	Transmission Electron Microscope
XRD	X-Ray Diffraction

Abstract

Nowadays, with the fast development of science and technology, we require more advanced material. Nanomaterials, having unique, beneficial chemical, physical, and mechanical properties, nanomaterials have been studied long times ago from the 1980s but its applications were very limited still. In recent decades, the nanomaterials have been successfully commercialized using different manufacturing processes, and can be used in a variety of industrial products, bio-medical and healthcare, etc.

Bimetallic nanoparticles (BNPs) are the nanometer-sized solid particle that formed by the combination of two different metals. The bimetallic nanoparticles have attracted huge attention as compared to monometallic nanoparticles in both technological and scientific view because BNPs show better properties.

Because of the remarkable properties and performance of iron (Fe) - copper (Cu) alloys, there are a lot of research study on the synthesis and applications of these materials. Even though their atomic radiuses are similar, the Fe and Cu are practically immiscible in the equilibrium state. As non-equilibrium solid solutions, the metastable Fe-Cu alloys can be synthesized by special methods such as rapid quenching, vapor deposition, sputtering, ion-beam mixing, and mechanical alloying. The complexity of those methods (multiple steps, low productivity, high cost and non-eco-friendly) can be crucial problem for industrial applications.

Electrical explosion of wire (EEW) is well known as an effective method for synthesis metallic and alloy nanoparticles. By explosive destruction of metal wires, materials of the wires turn into particles with nanosized range (10 – 100 nm). The extremely non-equilibrium conditions

of EEW can cause some interesting properties of the nanopowders. In addition, fabrication by the EEW can be a simple and economical process, lead to more applications in industrial.

In this study, Fe-Cu nanoparticles was fabricated by electrical explosion of wires. Powder shape and size distribution and alloying state will be analyzed and discussed according to the conditions of EEW. Fe nanoparticles, Cu nanoparticles, Fe and Cu mixed nanoparticles were also be prepared to be analyzed and compared with experimental conditions.

Chapter 1 - Introduction

Throughout history, the development of human society is closely linked to the development of materials. From the very beginning, we know how to use nature material in daily life. Human built houses, clothes and hunting tools from resources available in the wild. Started at Stone Age, human used stone to create tools to increase productivity. The oldest evidence of stone tool is a fossilized with is 3.4 million years old, were found in Ethiopia. Later, with many exposed copper ores, human create a new alloy, started the Bronze Age. It started first at Middle East, around 3300 BC. Meanwhile, the Bronze Age at Western Europe took place around 2000 BC, more than 1000 years later. Afterward, in 1200 BC, the use of iron marked the transition to the Iron Age. It can be clearly seen that the three great ages of mankind are all associated with the discovery and use a of new advanced material, therefrom we can notice the extremely important role of materials in human development. The evolution of material science is a significant premise to create breakthroughs in new technology development. Therefore, finding and producing new advanced materials are necessary steps towards the future.

In addition to discovering a new material, combining two metals to form an alloy is also an essential step in material enhancement. Back in Bronze Age, copper alone is too soft to be a tool. But by alloying, put tin into the material, it created bronze. The new alloy is much harder than copper alone, leading to a huge change in the way human use materials. The same things happen in the Iron Age. Compare to copper, iron is an outstanding metal for creating tools. But human do not stop there, we continue to create steel from iron. However, before 1850, steel was still a very expensive product with extremely limited application. They were mostly used for swords, tools and cutlery, while all large metal structures were made of wrought or cast iron. But, thanks to the

scientific breakthrough in the 1850s, with an advanced process, steel could be produced in large quantities and at low prices. Steel has become the most popular material in the world and a major component in construction and mechanical engineering. We can conclude that alloying is a simple but extremely effective way of finding more advanced materials.

Nanomaterials are gradually becoming favored materials for many researchers. With very small size, under 100 nm, nanomaterials have the properties that cannot be achieved by normal size materials. Among those properties, the most remarkable features of nanomaterials are their unique physical and chemical properties. Nanoparticle is a branch of nanomaterials, with all three external dimensions in the nanoscale range. Despite of being only a particle, these nanosized particles act like a complete unit. If the nanoparticle is made of a single metal, it is called monometallic nanoparticle. Bimetallic nanoparticles are nanoparticles that included two different metal elements on them. Bimetallic nanoparticles can be considered as an advanced alloy based on nanoparticles from two base metals. Because it is a nanoparticle, BNP will have unique nano properties as other nanoparticles. Also, we can study the promise new properties from combining two metals.

Iron and its alloys are used in many aspects of life including magnetic materials. However, when being alloyed, the magnetism of iron decreases quickly, limiting its application. However, the Fe-Cu alloy is very special, it maintains the magnetism of iron in the alloy even with a large amount of Cu in the alloy. Therefore, the Fe-Cu alloys have become a prospect for creating magnetic iron alloy materials.

Herein, the Fe-Cu bimetallic nanoparticles were synthesized by using EEW for twisted Fe-Cu wires in ethanol. The composition of the alloy could be change simply by changing the numbers

or wires twisted with each metal. We also synthesized iron, copper and their mixed nanopowders for comparison purposes.

Chapter 2 - Literature Review

2.1. Nanomaterials

Nanotechnology is a rapidly growing field of scientific where researchers study about nanomaterials, defined as extremely small solid particles [1]. With typical size in range of 1 to 100 nm, nanomaterials can have enormous specific surface area which lead to many unique physical and chemical properties [2]. The nanomaterials have boundless application across many science fields, such as physics, chemistry, biology, engineering and especially materials science. Slowly but surely, the nanomaterials are becoming commercialized and starting to emerge as essential commodities [3].

2.1.1. Nanoparticles

Nanoparticles (NPs) are defined as particles with all three external dimensions in the nanoscale (<100 nm) range, with no significantly different between longest and shortest axes. These nanosized particles act like a complete unit with either novel or superior properties that are significantly different and not attainable by conventional bulk materials [4]. The size of nanomaterials usually be limited between 10 and 100 nm by many researchers [5].

Nanoparticles undertake an important role in our day life nowadays. Human consume sunscreen products daily, but not everyone knows that titanium dioxide (TiO_2) nanoparticles are one of the most essential components of them [6]. With TiO_2 nanoparticles, only visible sunlight is allowed to pass through the skin and the harmful ultraviolet rays are blocked efficiently. Other nanoparticles are used in many applications depending upon their properties.

Preparation of nanoparticles can be done by two general approaches: top-down approach and bottom-up approach, as shown in Fig.1. [7, 8]. In the top-down approach, the process refers to the disintegration from a larger parent superstructure to create a nanostructure [9]. Presently, this approach is dominantly used in industry for making materials, especially in semiconductor industry [10, 11]. However, the bottom-up approach is most used for the preparation of the nanoparticles. Contrary to the top-down approach, the bottom-up involves crafting structure from atomic level to the nano-scale level, atom by atom, similar to a house is built brick by brick [12-15]. Because the NPs are synthesized from relatively simpler substances, this approach is also known as building up approach. Typical examples of this are sedimentation and reduction techniques, such as: sol gel, green synthesis, spinning, and biochemical synthesis.

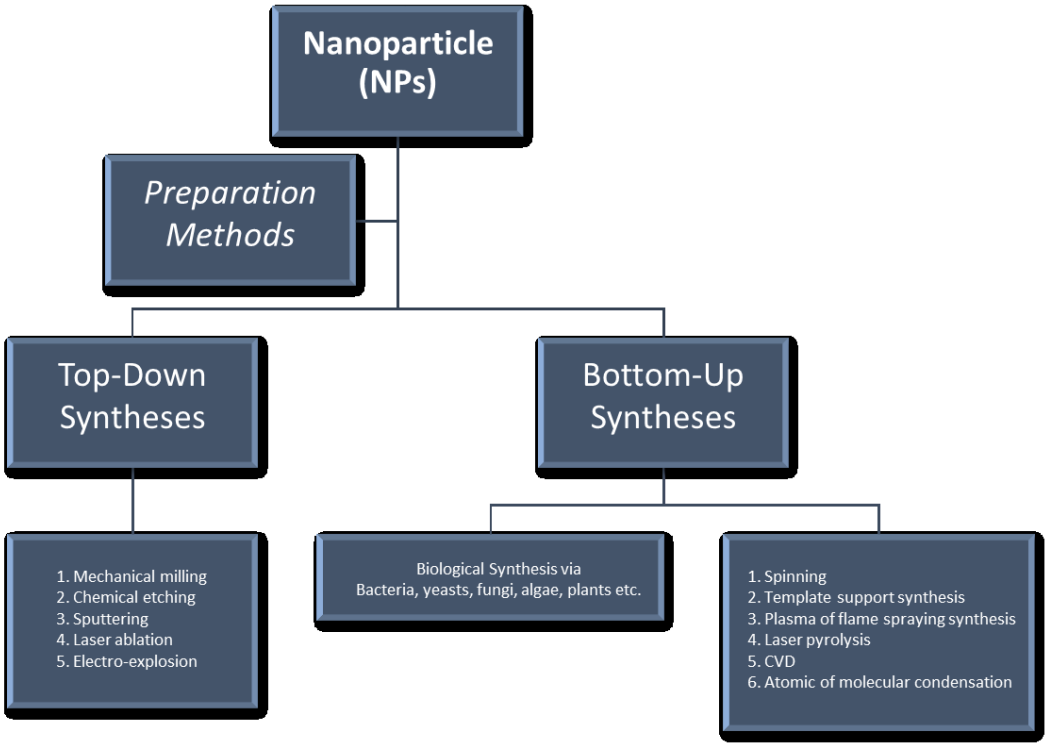

Fig. 1. Typical synthetic methods for NPs for the top-down and bottom-up approaches.

2.1.2. Monometallic Nanoparticles

Monometallic nanoparticles (MNPs), as the name suggests, are nanoparticles that only made of a single metal. MNPs can be classified into magnetic, metallic and transition metal nanoparticles, etc. depend on the constituted metal atom. Each kind of MNPs has individual applications that suit its properties, and can be used for a number of applications such as in electronic, optical and catalysis, etc. For example, silver nanoparticles have been used widely as antimicrobial agents against a number of microorganisms such as Escherichia coli [16], Bacillus subtilis [17], Streptococcus pyogens [18], and Streptococcus mutans [19].

2.1.3. Bimetallic Nanoparticles

Composed of two different metal elements, bimetallic nanoparticles (BNPs) have been attracted more attention than monometallic nanoparticles from both scientific and technological viewpoints [20]. The BNPs have potential unique electrocatalytic [21-23], catalytic [24-28], magnetic [24, 29, 30], and optical properties [24, 31] that MNPs can not acquire [32]. The properties of the BNPs are determined by composed metals and their nanometric size, may not only be the combination of the properties related to two individual metals, but also have potential to form novel properties due to the interaction between two components. The distribution and organization of each alloys will be depended on the synthesis methods used in the preparation of BNPs, can be mixed alloys, random alloys, subclusters, etc., as shown in Fig. 2 [24, 32, 33].

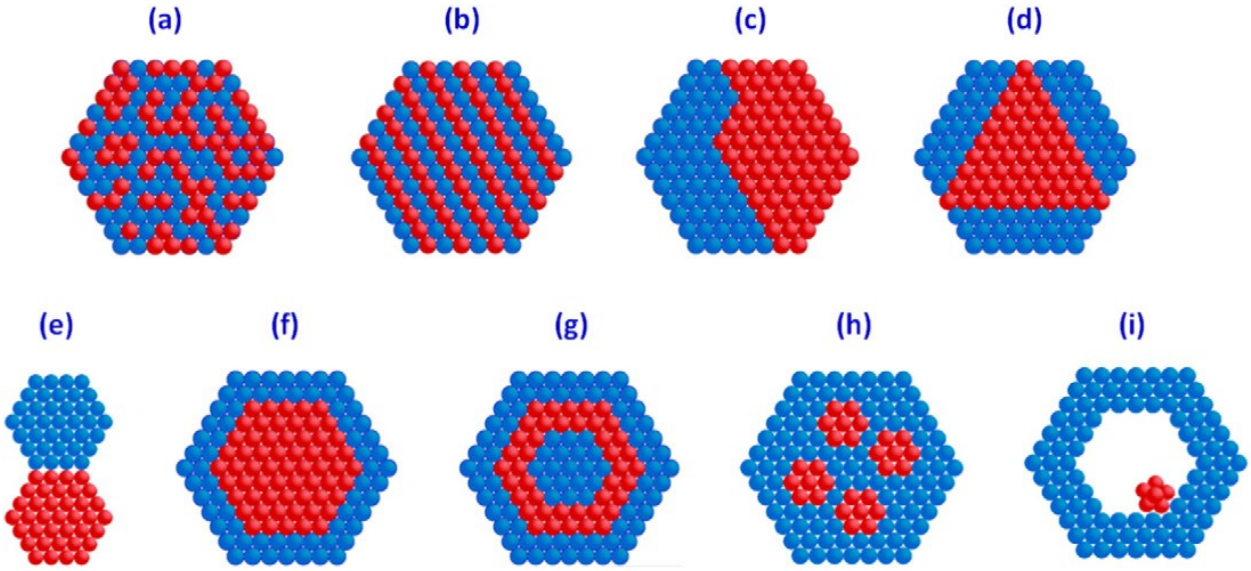

Fig. 2. Structures of bimetallic nanoparticles: (a) mixed alloys; (b) random alloys; (c) subclusters with two interfaces (d) subclusters with three interfaces; (e) subclusters with small number of A–B bonds; (f) core–shell nanoparticles; (g) multishell core–shell nanoparticles; (h) multiple small core material coated by single shell material, (i) movable core within hollow shell material.

Lately, there are research works about the production of BNPs, mostly is antibacterial BNPs with the presence of silver as the particle core or shell. However, because silver nanoparticles have cytotoxicity and genotoxicity properties, application of the BNPs containing silver is very limited [34]. Therefore, science community tend to shift their research to other promise BNPs. Recently results show that the applying of the BNPs containing biologically active metals, such as Fe and Cu, can be truly prospective [35].

2.2. Fe-Cu Alloys

Fe-Cu alloys are very unique magnetic materials. Normally, the magnetic moment of Fe atom is quickly reduced by alloying but it remains nearly constant up to very high concentrations of Cu in Fe-Cu alloys. That unique magnetic properties, accompanied by its high strength and attractive electric and thermal properties make the Fe-Cu alloys system become very attractive for scientific research community [36-40]. In term of Fe-Cu alloys, bimetallic particles and nanoparticles consisting Fe and Cu components have been used in environmental and medical applications thanks to the high removal capacities for pollutant removal, excellent antibacterial and corrosive resistance properties [41]. But similar to other metastable alloy systems, because of its positive energy of mixing (around 13 kJ/mol for the Fe-Cu system), Fe-Cu alloys are very limited miscibility and their synthesis suffers for that main drawback [42, 43]. In fact, the Fe-Cu system is nearly immiscible in equilibrium at room temperature and up to 600^{o}C [44, 45], the fabrication of this material has the difficulties in processing. However, the usefulness in this material's application still attracts attention of researchers and manufactures, therefore, several techniques have been studied and applied to synthesis the Fe-Cu alloys included rapid quenching [46], vapor deposition [47, 48], sputtering [49], ion-beam mixing [50], mechanical alloying [51, 52], and high-pressure torsion [53]. Thus, developing a new method for synthesizing nanostructured Fe–Cu alloys is a critical challenge for all researcher. From an economics viewpoint, proposing a possible route which can simply manufacture nanostructured Fe–Cu alloys, the ones with low cost but still good quality is needed.

2.3 Fabrication of Fe-Cu Alloys

2.3.1. Rapid Quenching

In the past, Klement, W. et al. proposed using rapid quenching to synthesize Fe-Cu metastable alloys [46]. They prepared homogeneous alloys by casting and sintering from 99% purity elements. The special thing about this quenching technique is that all iron alloys were completely covered with argon while at elevated temperatures. This research had successful obtained single-phase Fe-Cu solid solutions.

2.3.2. Vapor Deposition

Vapor deposition, here is Physical vapor deposition (PVD), is described as a variety of vacuum deposition methods used to produce high quality, high performance, solid materials like thin film and coating. The typical characteristic of the PVD process is that the material will be vaporized then condensed back into a thin film phase. Fe-Cu solid solutions were synthesized using physical vapor deposition (PVD) and analyzed by Chien, C. et al [48]. The products obtained were thin film with a thickness of 8-15 μm.

2.3.3. Sputtering

Sputtering and evaporation are the most common PVD processes, they have been widely used in semiconductor industry to produce thin film. Sputtering is a process where materials are ejected from a “target” that is a source onto a “substrate” by using high energy external stimuli. Despite being able to produce very high purity nanoparticles, this method suffers from certain drawbacks such as less control over the particle morphology and quite high energy consumption

[5]. Also, because of requiring high temperature, this method can be acutely harmful and causing skin diseases.

2.3.4. Ion-Beam Mixing

Ion beam mixing is a process that materials under ion irradiation undergo significant atomic rearrangement [54]. It could be applied as a process for adhering two multilayers, create the connection between a substrate and a deposited surface layer. Ion beam mixing is a potential alternative way to synthesis non-equilibrium or metastable alloys and intermetallic compounds. The Fe-Cu metastable incommensurate phase was prepared by ion beam mixing of multilayer films with 300 keV Xe^{+} ions at room temperature [50]. They used a vacuum electron gun system to depositing pure constituent metals (Fe, Cu) onto inert substrates to create multilayer films. The atomic concentrations of Fe-Cu films were adjusted by changing the thickness of metal layers, and the total thickness of the films were chosen to be about 60 nm.

2.4. Electrical Explosion of Wire

The electrical explosion of wire (EEW) is a process of explosive destruction of metal wires under the action of great density current ($> 10^{10}$ A/m^2) [55]. This process is accompanied by scattering products, shock waves and electromagnetic radiation. EEW is characterized by the following peculiarities: time of explosion is 10^{-5} - 10^{-8} s; temperature at the moment of explosion can reach the value more than 10^4 K; pressure ~10^9 Pa; velocity of product recession is from 1000 to 5000 m/s [55]. This technique has attracted attention for fabrication of various metallic nanopowders due to the simple and low-cost processing [56]. EEW can be used to cheaply and

efficiently produce nanoparticles at a rate of 50-300 grams per hour and at a purity of above 99%. The particles can be as small as 10 nm but are most commonly below 100 nm in diameter. This is a simply physical process and a suitable top-down approach for nanosized powder production. Material of the wire transmutes into the nanoscale particles in accordance with certain conditions. Extremely nonequilibrium condition of EEW cause some unusual properties of nanopowders. They are steady against oxidation and sintering at room temperature and characterized with high diffusion activity at the heating [51].

Chapter 3 - Experimental Details

3.1. Materials

Iron and copper wires were used for this research. Iron wire and copper wire with diameter of 0.2 mm was provided (Fig. 3). The purity of both iron and copper wire are ~99%. The physical properties of Fe and Cu are summarized in the Table 1. Ethanol was used as solution for the explosions. All materials were commercially available and used as the received materials without further purification.

Iron wire (0.2 mm)

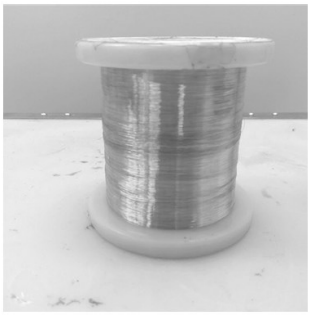

Copper wire (0.2 mm)

Fig. 3. The as-received Iron wire and Copper wire

Table 1. Physical properties of Iron and Copper

	Density	***Melt. temp***	***Boil. temp***	***Atomic radius***	***Atomic volume***	***Thermal cond.***	***Electrical cond.***
	ρ, g/cm^3	*T_m, K*	*T_b, K*	*Å*	*cc/mol*	*λ, W/m.K*	*σ, 10^7 S/m*
Iron	7.87	1811	3133	1.26	7.1	80.4	1.04
Copper	8.96	1358	2840	1.28	7.1	401	5.98

3.2. Experimental Procedures

The iron and copper nanoparticles were prepared by exploding 0.2 mm ø iron wires (99% pure) and 0.2 mm ø copper wires (99% pure) in ethanol, respectively. These two powders also be taken to mix together in one solution to get the Fe-Cu mixed nanoparticles. In other experiment, Fe wires (0.2 mm ø) and Cu wires (0.2 mm ø) were twisted together (with the ratio 1:1 and 2:1) in order to synthesis Fe/Cu and Fe_2/Cu nanoparticles (Fig. 4). The composition content of the metals in the twisted wire was calculated by the specific density and the diameters of the wires (Table 2).

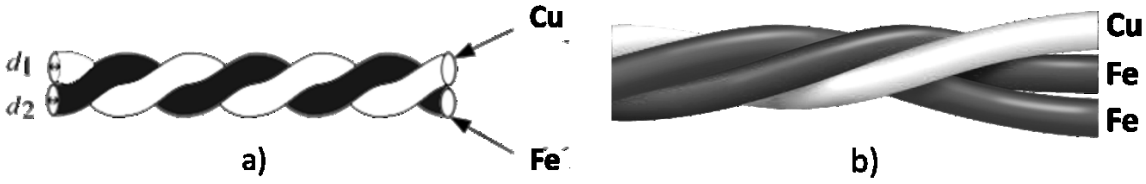

Fig. 4. Copper and Iron wires were twisted together a) Fe/Cu (1-1) b) Fe_2/Cu (2-1)

Table 2. Metal wire composition

	Name	*Fe (%)*	*Cu (%)*	*Twisted*
1	Fe	100	0	x
2	Cu	0	100	x
3	Fe-Cu	50	50	x
4	Fe/Cu	47.17	52.83	o
5	Fe_2/Cu	63.46	36.54	o

Wires were cleaned with ethanol to remove surface contaminants before experiments. The wire characteristics are given in Table 3 (T_m is the metal melting temperature, ρ is the specific metal density, d is the wire diameter, l is the wire length).

Table 3. Metal wire characteristics

Wire metals	T_m, K	ρ, g/cm^3	***d, mm***	***l, mm***
Fe	1811	7.87	0.2	40
Cu	1358	8.96	0.2	40

The schematic steps of the experiment procedure were presented in Fig. 5. All the experiments were conducted in the EEW machine with an ethanol solution bath at room temperature condition (Fig. 6). The applied voltage and the capacitance of the exploding circuit across the 4-mm-long wire was 3.42 kV and 30μF, respectively. After the explosion, the powders were collected from solutions by drying at room temperature under vacuum condition for 24 hours.

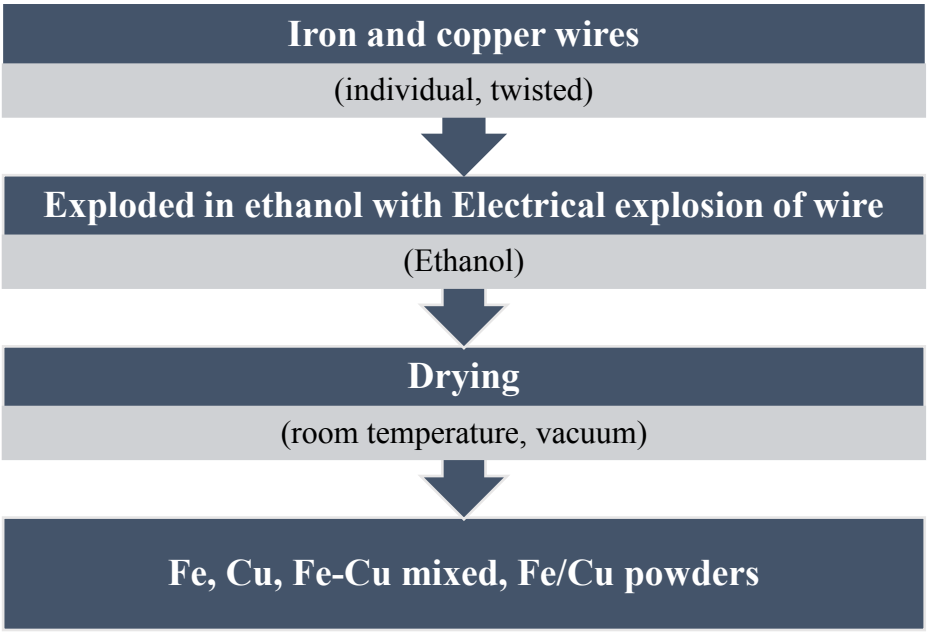

Fig. 5. Schematic diagram showing experimental steps for processing

Electrical explosion of wire

- Cu wires : 0.2 mm
- Fe wires : 0.2 mm
- Charging Voltage : 3.42 kV
- Capacitance : 30 μF
- Liquid : Ethanol
- Liquid content : 3500 mL
- Room temperature

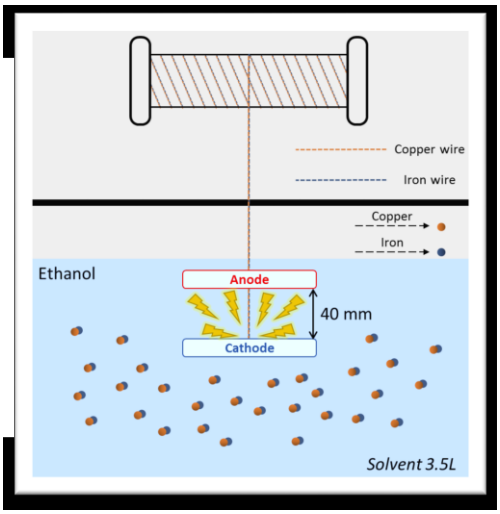

Fig. 6. Conditions used for the electrical explosion of wire process

3.3. Characterization Analyses

3.3.1. X-Ray Diffraction

X-ray diffraction is an essential tool in material analysis, an effective technique to identify the phases present in a sample. With simple crystal structures, metals always have few peaks in the diffraction pattern. As defined, the space lattice is a regular array of points in space, and the crystal structure is formed when a basis of atoms is attached identically to every lattice point. So, crystal can be considered as regular arrays of atoms and X-ray can be considered as waves of electromagnetic radiation. In the method, when a wave of X-ray strikes a single crystal, atoms' electrons scatter it, producing scattered waves. A regular array of scatters produces a regular of spherical waves. When they land on the detector, these waves make a diffraction pattern of spots, the strength and angles of these waves are recorded as the crystal is gradually rotated. Although these waves cancel one another out in most directions through destructive interference, they add constructively in a few specific directions determined by Bragg's law:

$$2d \sin\theta = n\,\lambda$$

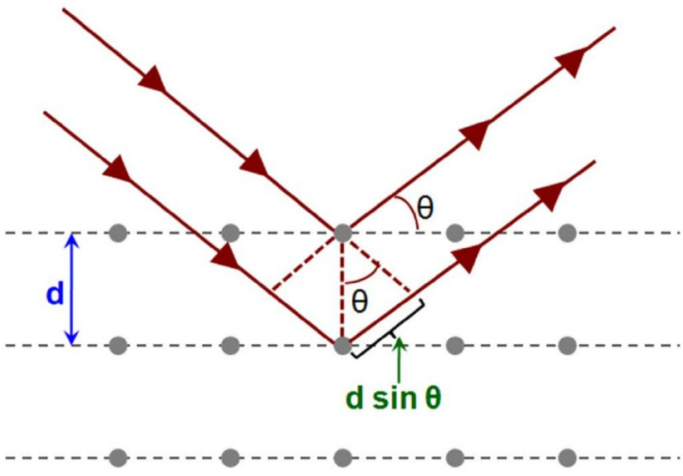

Fig. 7. Diffraction of X-ray by planes of atoms

Here d is the spacing between diffracting planes, θ is the incident angle, n is any integer, and λ is the wavelength of the beam. Each spot is called a "reflection", since it corresponds to the reflection of the X-ray. For single crystals of sufficient purity and regularity, X-ray diffraction data can determine the mean chemical bond lengths to within a few thousandths of an angstrom and angles to within a few tenths of a degree.

Fig. 8. Ultima IV X-ray Diffractometer

In this work, the XRD measurement was carried out by using Ultima IV X-ray diffractometer (Rigaku). The sample were analyzed with Cu $K\alpha$ radiation (λ = 1.5406 Å) at a scan rate of 1^{o}/minute (Fig. 8). The diffraction data were provided using the software DIFFRAC-AT connected with the instrument.

3.3.2. Scanning Electron Microscope

A scanning electron microscope (SEM) is a microscope technique in which a beam of electrons is scanned the surface of a sample to form an image. As the electron impact with atoms in the sample, various signals are produced and collected. Those signals contain information about the surface topography and composition of the sample. Normally, the signal has been mentioned are secondary electrons that emitted by atoms excited by the electron beam. They can be detected using Everhart-Thornley detector. Depending on the used model, SEM machine can achieve resolution better than 1 nanometer.

Fig. 9. JSM Field Emission Scanning Electron Microscope

In this experiment, the microstructure and chemical elements of the powders were observed and analyzed by Field-emission scanning electron microscope (FE-SEM, JEOL JSM-6500F) equip with Energy-dispersive spectroscope (EDS) (Fig. 9). The samples were prepared with medium platinum coating and the experiments are carried out in both the secondary and backscattering electron imaging mode at 15kV.

3.3.3. Transmission Electron Microscope

A transmission electron microscope (TEM) is an electron microscope that produces images using a focused beam of electrons to transmit through a specimen. In order to successfully transmit the electrons, they usually use an ultrathin section less than 100 nm thick or a suspension on a grid as a specimen. While the beam is transmitted through the specimen, the interaction between the electrons and the sample create a TEM image. Due to the smaller de Broglie wavelength of electrons, transmission electron microscopes would certainly receive high-resolution image that cannot achieved by light microscopes. Therefore, TEM has become a major analytical method in physical science, chemistry and biology.

Fig. 10. Transmission Electron Microscope

The TEM microscopic analysis of samples were carried out with JEOL JEM-2100F, operating at 150 kV (Fig. 10). The samples were carefully prepared with holey carbon coated grids for experimental investigation.

3.3.4. Turbiscan Method

Turbiscan technology consists in measuring the backscattering and transmission intensities versus the sample height in order to detect particle size change (coalescence, flocculation) and

phase separation (sedimentation, creaming). This technique uses the multiple light scattering method to characterize concentrated liquid dispersions without dilution.

Chapter 4 - Experimental Results and Discussion

4.1. Morphology Analysis

4.1.1. Exploded Iron and Copper Wires

The morphology and size of as-prepared powders produced by EEW were investigated by FE-SEM. Fig. 11. and Fig. 12. show the FE-SEM images of exploded iron and exploded copper in ethanol. After drying step, the metal powders tend to stick together rather than being separated. But we can still see that the iron and copper powders were majorly spherical in shape with a very small amount of irregular shape particles. With a same condition, iron particles have bigger size than copper particles, their particle size distribution ranges from 50-200 nm and 10-100 nm, respectively.

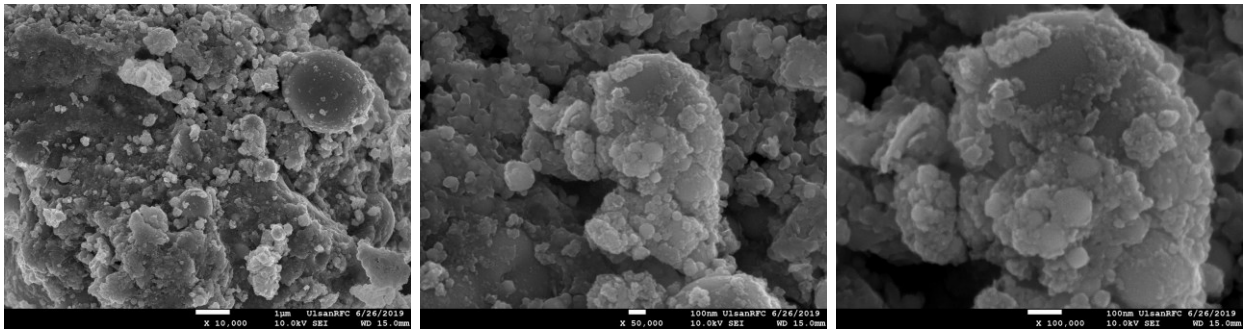

Fig. 11. FE-SEM images of iron nanoparticles prepared by EEW

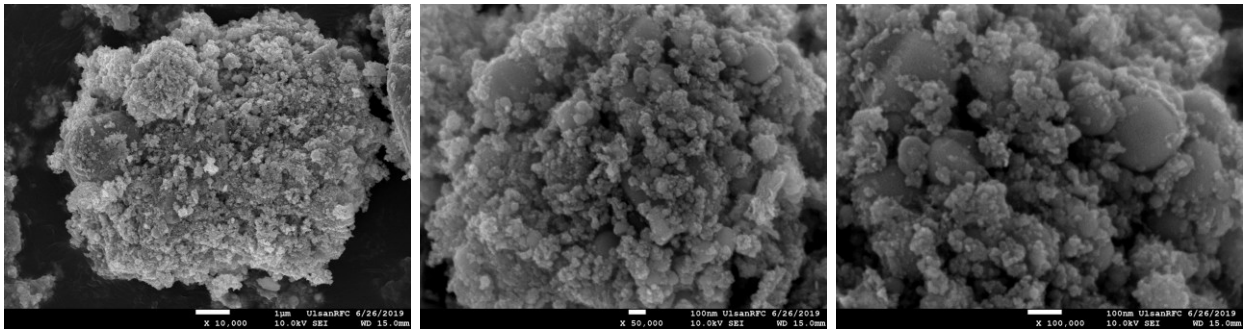

Fig. 12. FE-SEM images of copper nanoparticles prepared by EEW

Fig. 13 show the EDS images of iron and copper exploded in ethanol. As we can observe, there is a significant amount of oxygen in both samples, beside the original metal. The existence of oxygen can be explained by the formation of metal oxides during the experiment process. After the explosions, iron and copper nanoparticles reacted with oxygen to form the oxide film, covering the nanoparticles.

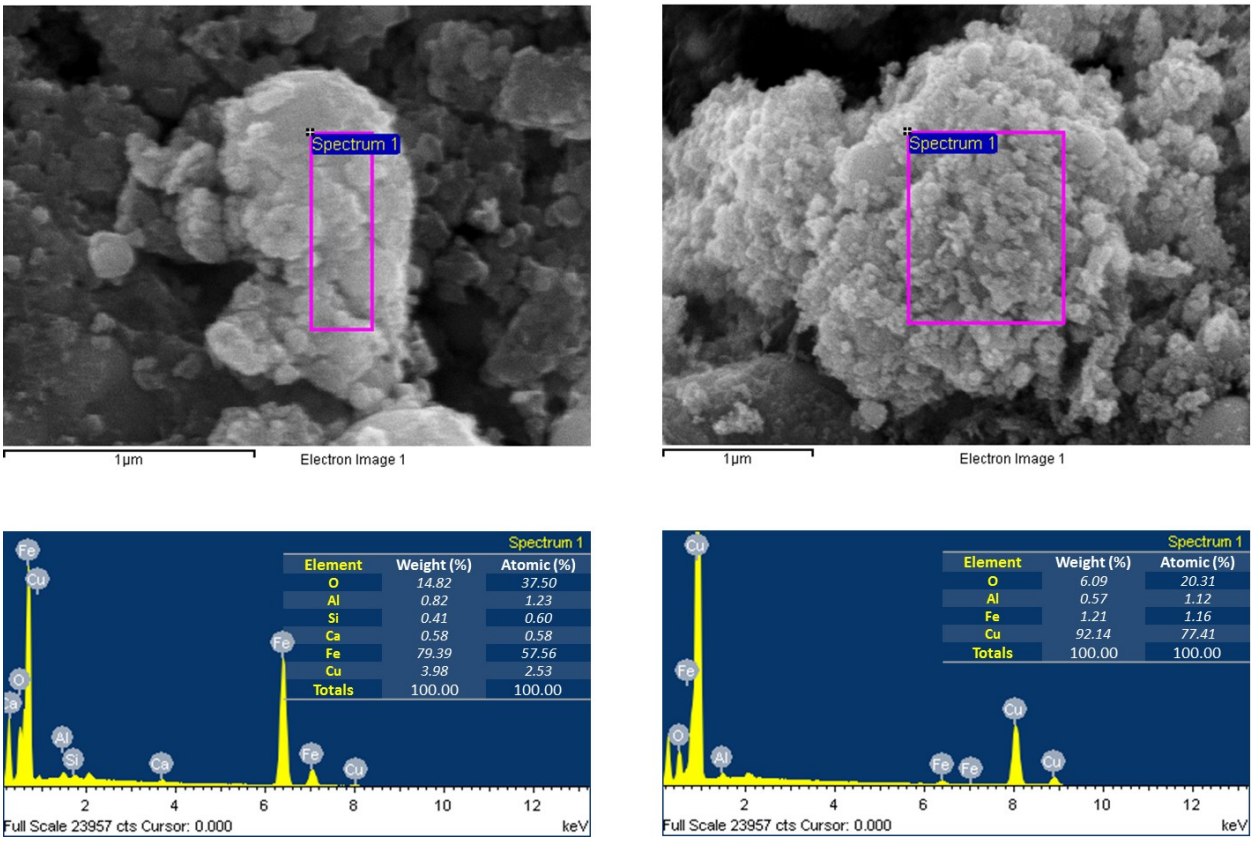

Fig. 13. EDS images of iron and copper nanoparticles prepared by EEW

In other experiment, as we can observed in Fig. 14, Fe and Cu mixed nanopowders have similar shape and size with Cu-only nanopowders. The particle size could be classified into two groups based on diameter as nanoparticles (with the diameters under 100 nm) and fine particles

(with the diameters slightly larger than 100 nm). This powder is the mixture of iron and copper powder, so we can know that some scattered particles (Fe) were covered by many smaller particles (Cu).

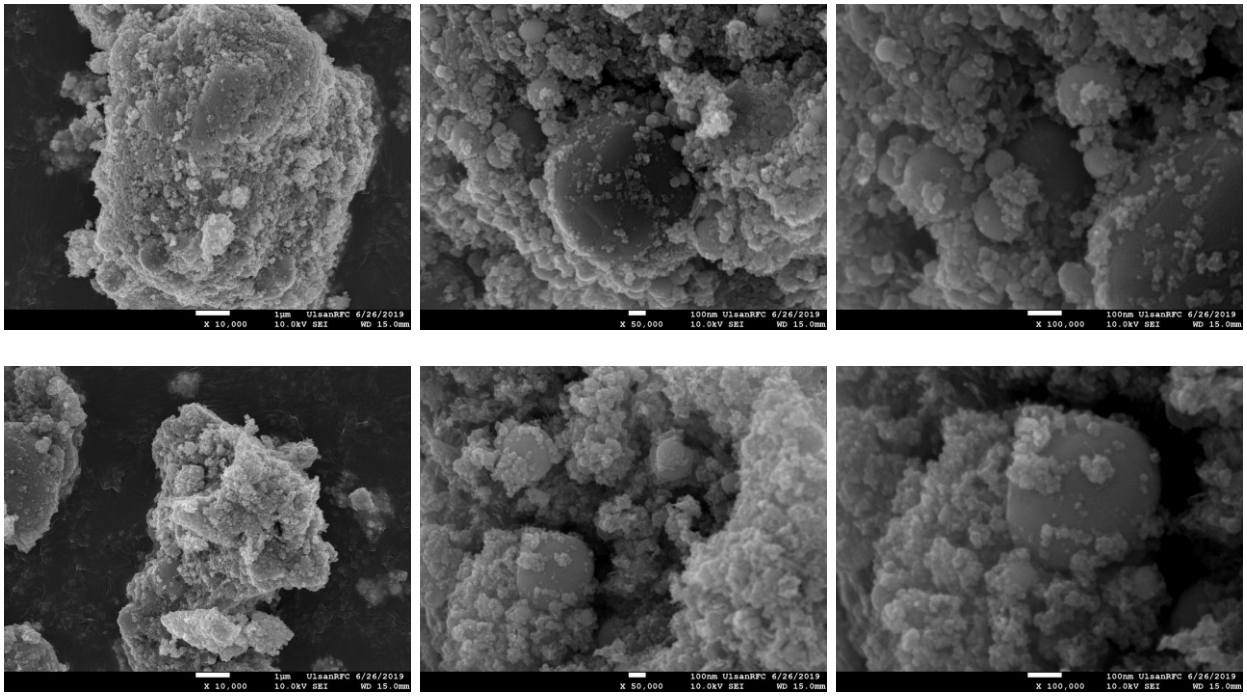

Fig. 14. FE-SEM images of Fe-Cu mixed nanoparticles prepared by EEW at magnifications

Fig. 15 show the EDS images of Fe-Cu mixed exploded in ethanol. Oxygen still exist in sample, similar to previous experiments. This is an affirmative of the creation of metal oxides in the product, and be confirmed by XRD results (Fig. 20). In EDS results, we can see that the percentage of Cu (~79%) is much more than Fe (~11%). It can be explained that many small particles of Cu have covered larger particles of Fe, affects the EDS results.

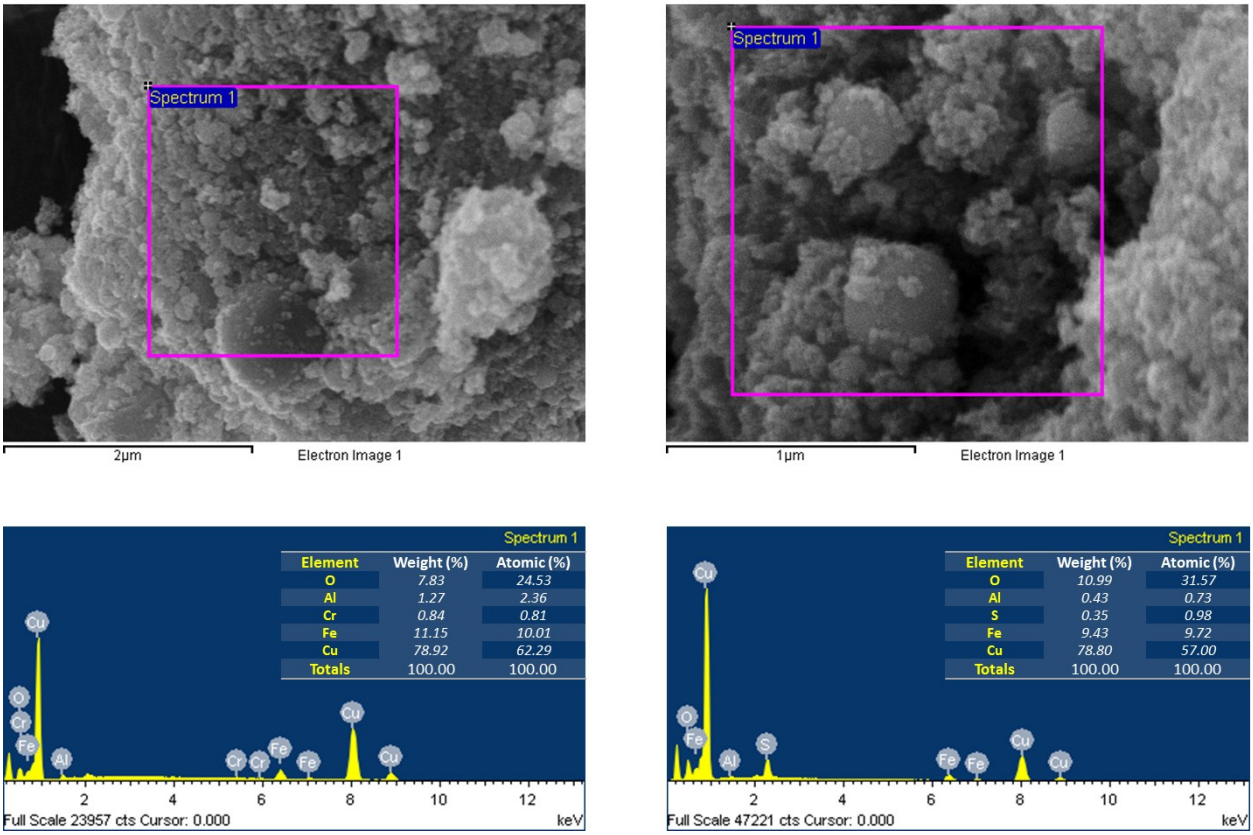

Fig. 15 EDS images of Fe-Cu mixed nanoparticles prepared by EEW

4.1.2. Exploded Iron-Copper Twisted Wires

When twisted wire together, both Fe_2/Cu particles and Fe/Cu particles can be observed in Fig. 16 and Fig. 17, respectively. Despite of the change on material composition, these two samples do not have much difference on morphology structure, their particles both have spherical shape and particle size spread from 50 to 120 nm Different to Fe-Cu mixed powder, the size of metal particles was not clearly split into two groups but spread evenly.

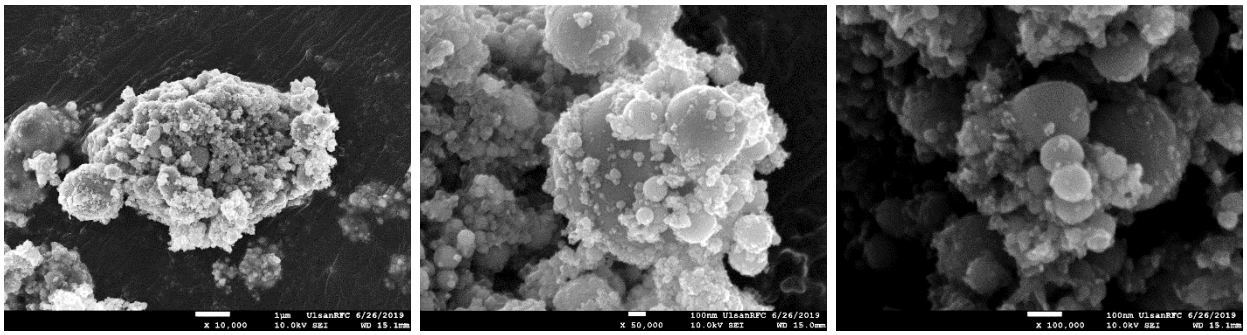

Fig. 16. FE-SEM images of Fe_2/Cu nanoparticles prepared by EEW

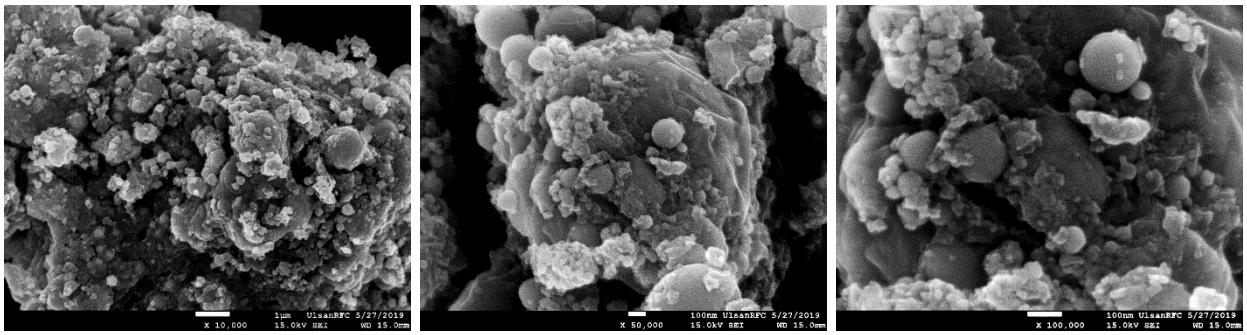

Fig. 17. FE-SEM images of Fe/Cu nanoparticles prepared by EEW

In Fig. 18 and Fig. 19, EDS images of Fe_2/Cu nanoparticles and Fe/Cu nanoparticles can be observed. We can notice the existence of a significant amount of carbon element in both samples. This amount of carbon come from the ethanol used for experimental solution. Because there is no reaction between carbon and metal in this experiment, the carbon exists in the form of layers covering the metal particles.

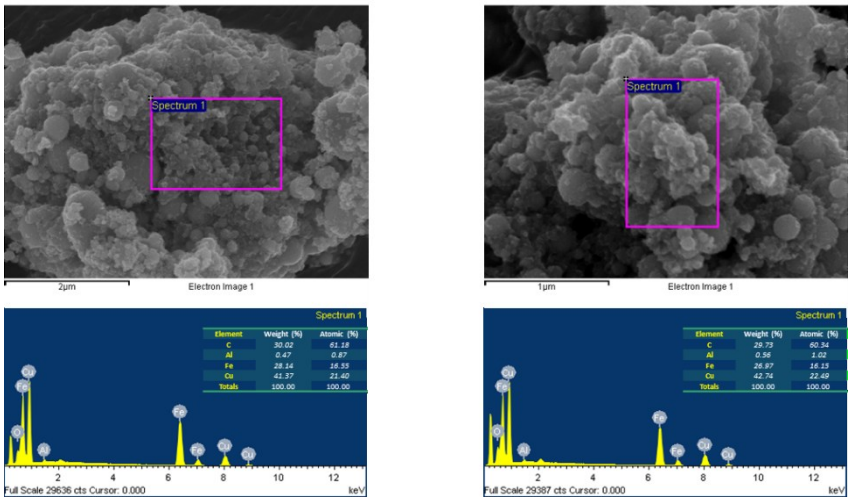

Fig. 18. EDS images of Fe_2/Cu nanoparticles prepared by EEW

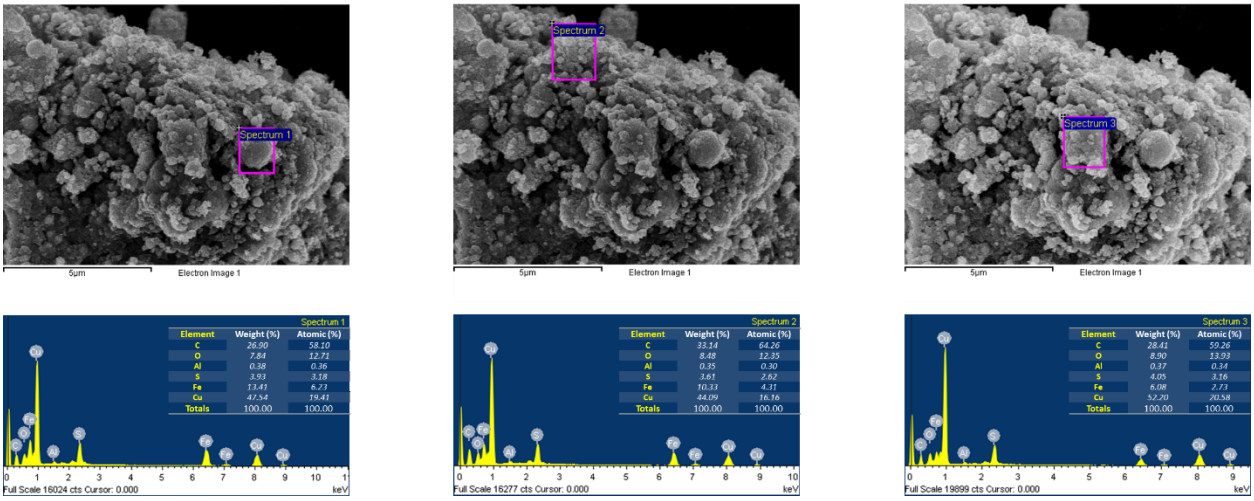

Fig. 19. EDS images of Fe/Cu nanoparticles prepared by EEW

The morphology and shape of the synthesized Fe/Cu nanopowders were also observed by TEM analysis, the results were presented in Fig. 20 and Fig. 21. It could be seen that the as-

prepared powders have a spherical form with the particles size was extensively spread from 10 to 200 nm. According to the TEM images, the particles size consists of big and small particles with a tendency increasing in the amount of the small one with the higher of Fe content in the twisted wires. This is attributed to the difference in the melting point and the electrical conductivity between Fe and Cu. The TEM images also reveals that there is a layer of material covered the particles after exploding which is confirmed graphitic carbon layer with the thickness is about 0.3 nm. The presence of the graphitic layer is attributed to the existence of the large amount of carbon element diluted in the ethanol solvent. The TEM results further supports the XRD analysis regarding the formation of bimetallic Fe/Cu particles. Thus, the high-resolution TEM images depict the lattice fringes of the phases as have observed through XRD pattern with the lattice spacing d = 0.2 nm which is the same with the lattice spacing of Cu and Fe.

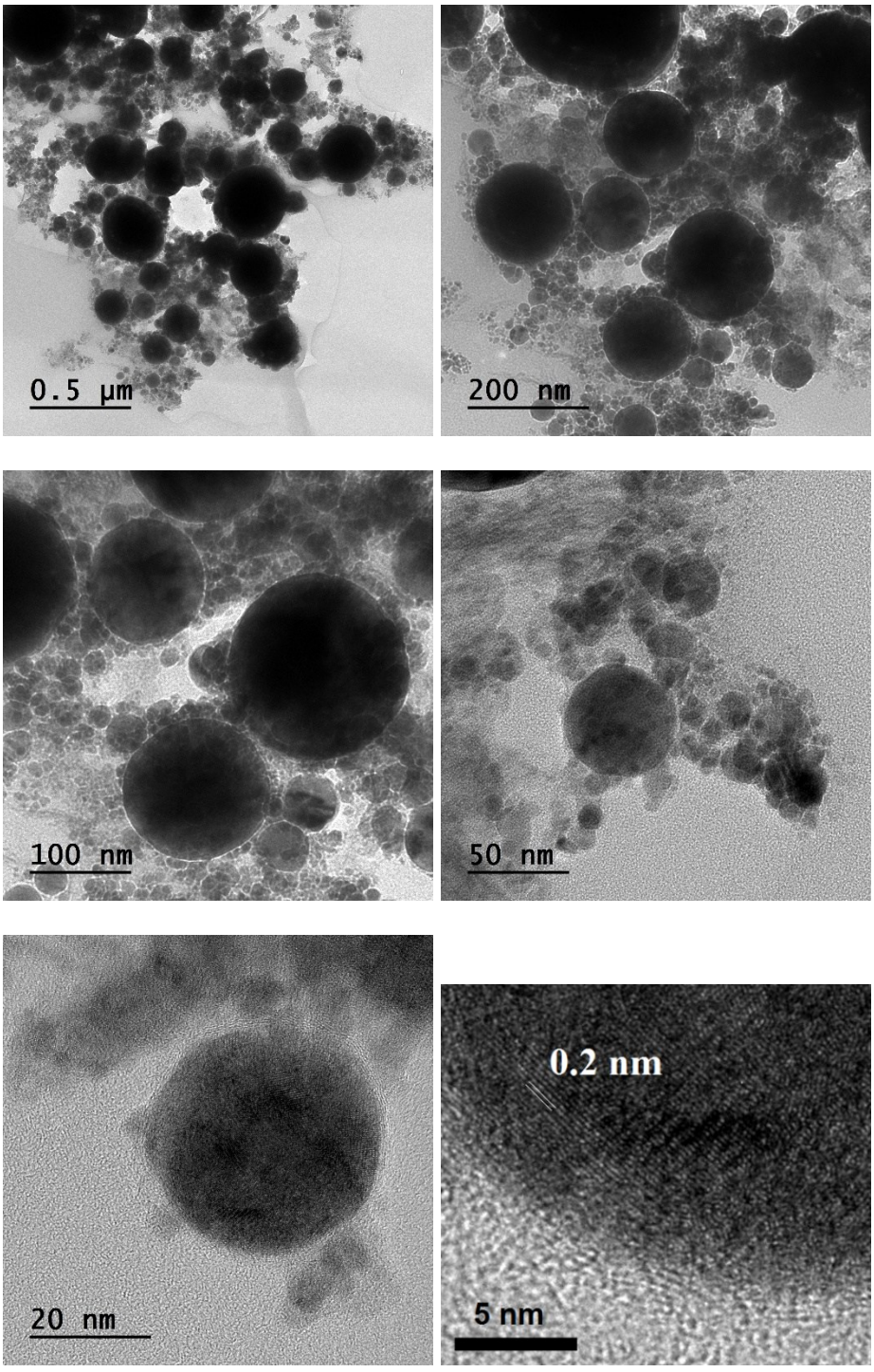

Fig. 20. TEM images of Fe_2/Cu nanoparticles prepared by EEW

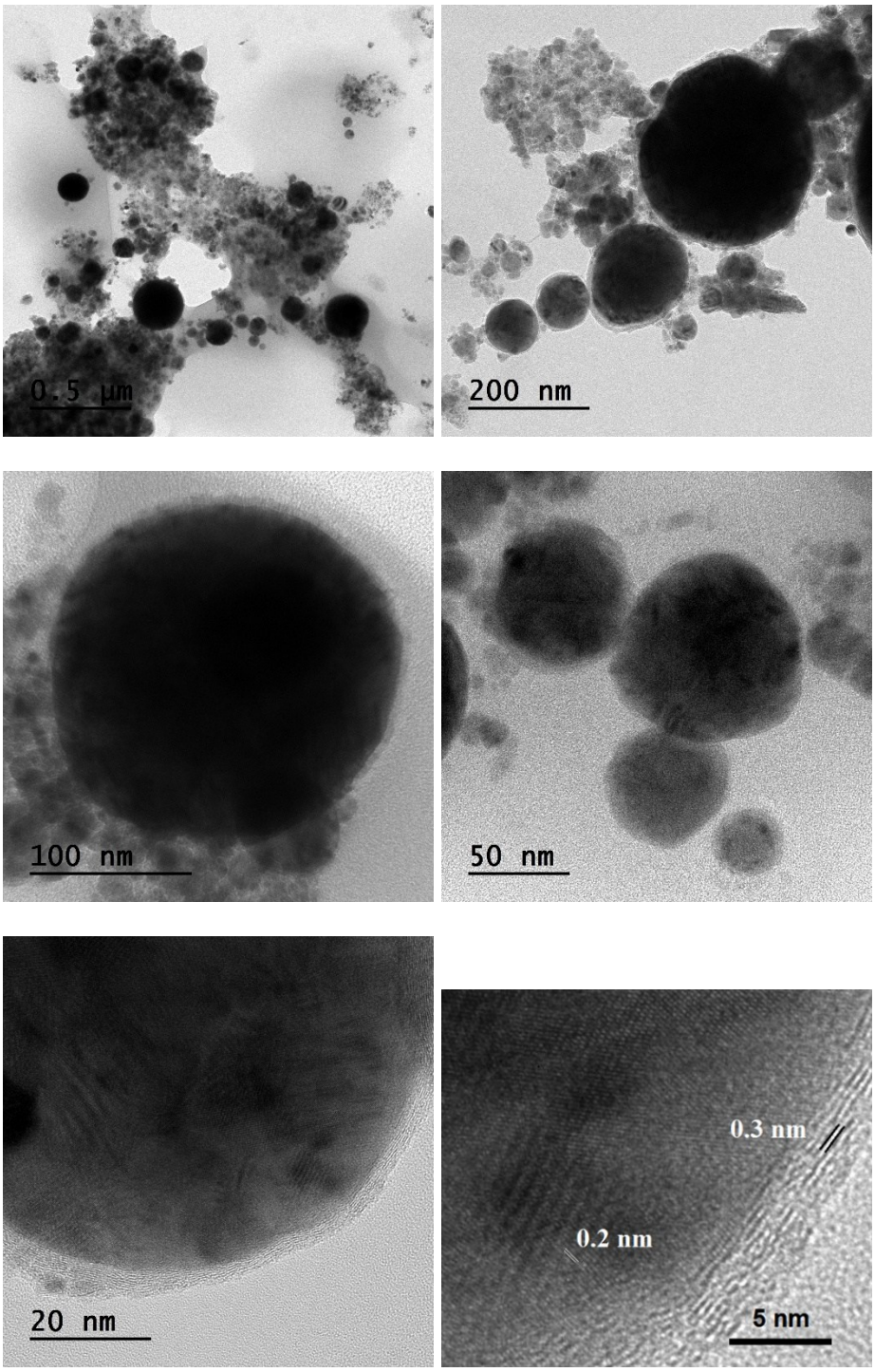

Fig. 21. TEM images of Fe/Cu nanoparticles prepared by EEW

4.2. Phase Analysis

4.2.1. Copper Wires

Fig. 22. show the x-ray diffraction patterns of copper powders exploded in DI water (a) and ethanol (b). With all samples, the XRD results show the major diffraction peaks at 43.24^o; 50.36^o; 74.06^o; and 89.86^o corresponding to (111), (200), (220), and (311) planes of the fcc structure of pure copper. Coexisted with pure Cu, there is also the presence of CuO and Cu_2O peaks in the patterns.

The appearance of CuO and Cu_2O in solutions could be explained by the interaction of copper particles with oxygen diluting in the liquid when Cu vapor condensed. The oxidation of copper could be expressed by the two following equations [57].

$$Cu + O_2 + H_2O \rightarrow Cu_2O \qquad (1)$$

$$Cu_2O + O_2 \rightarrow CuO \qquad (2)$$

According to these equations, ethanol could be considered as a proper environment for the (1) equation occurred, to synthesize CuO, but not suitable for continuing the formation of Cu_2O. Different to ethanol, in DI water solution, due to the existence of H_2O and diluted oxygen, become a suitable environment for the (2) equation. First, the surface of copper particles was initially oxidized and quickly formed Cu_2O shell (1). Then, the oxide shell was infiltrated by oxygen, continue to create CuO (2). That is the way the phase of CuO and Cu_2O were created.

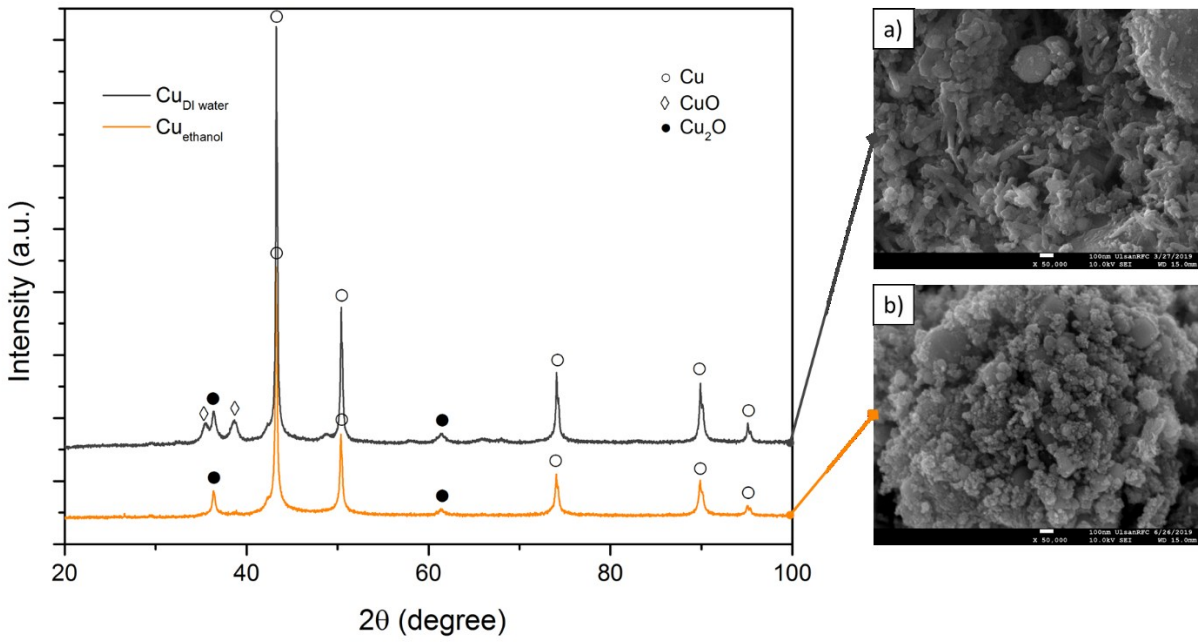

Fig. 22. XRD patterns of exploded Copper in DI water (a) and in ethanol (b)

4.2.2. Fe, Cu, Fe/Cu Phase

For determination of the phase structure of the exploded products the XRD analysis was conducted. Fig. 23. shows the XRD pattern of the as-prepared powders. According to the result, the XRD pattern of the synthesized Fe powders shows a dominant peak at 2θ = 44,58º which corresponds to the (110) plane of the face centered cubic (fcc) with a little percentage of iron oxide (Fe_2O_3) that could be observed by small peaks at 2θ = 64,98º, and 82.49º [19]. With as-exploded Cu powder, the XRD pattern shows mainly the peaks are in good conformity with the pure cubic copper phase with the peak positions at 2θ = 43.24º, 50.36º, 74.04º, and 89.86º. However, the other peaks corresponding to the presence of Cu_2O phase (at 2θ = 36.36º, 42.30º, and 61.32º) were also observed. The appearance of iron oxide and copper oxide phase in the as-exploded powders is

attributed to the interaction of Fe and Cu with oxygen diluting in the solvent during exploding stage.

According to XRD peak analyses of synthesized Fe/Cu powders ($Fe_{47}Cu_{53}$), the major reflections have been attributed to copper and iron, however, the peak of Fe were weakened by copper implantation. In addition, it is found that the new peaks belong to new phases of Cu bearing $Fe_{0.1}Cu_{0.9}$, $Fe_{0.2}Cu_{0.8}$, $Fe_{0.6}Cu_{0.4}$ and Fe_4Cu_3 were examined. The phases of $Fe_{0.2}Cu_{0.8}$ can be clearly observed the three well-defined peaks at $2\theta = 43.26^o$, 50.38^o, 74.04^o. The other peaks at $2\theta = 89.82^o$ and $2\theta = 95.06^o$ is attributed to the presence of the phase of $Fe_{0.1}$ $Cu_{0.9}$. Also, there are other small peaks at $2\theta = 44.68^o$ and $2\theta = 46.02^o$, correspond to the phases of Fe_4Cu_3 and $Fe_{0.4}Cu_{0.6}$, respectively. This result demonstrates that the bimetallic Fe/Cu particles were synthesized successfully by explosion of the initial twisted wires in the ethanol condition.

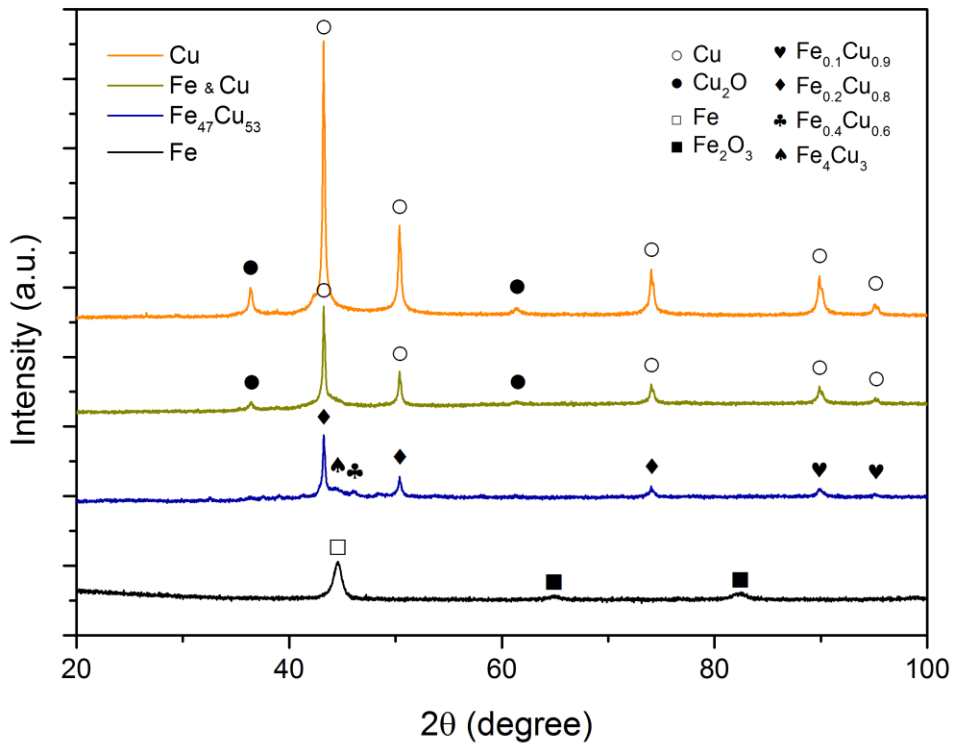

Fig. 23. XRD patterns of exploded Iron, exploded Copper, exploded Iron and Copper, exploded Iron and Copper (twisted)

4.2.3. Iron-Copper Twisted Wires

Fig. 24. show XRD patterns of Fe/Cu and Fe_2/Cu samples. As we can observe, although the peaks look similar for two samples, there still be some minor difference. The peak at $2\theta = 46.02^o$ represented $Fe_{0.4}Cu_{0.6}$ only appeared in Fe/Cu ($Fe_{47}Cu_{53}$) sample, not in the other. Base on this result, it can be concluded that the input composition will determines the alloy synthesis phases.

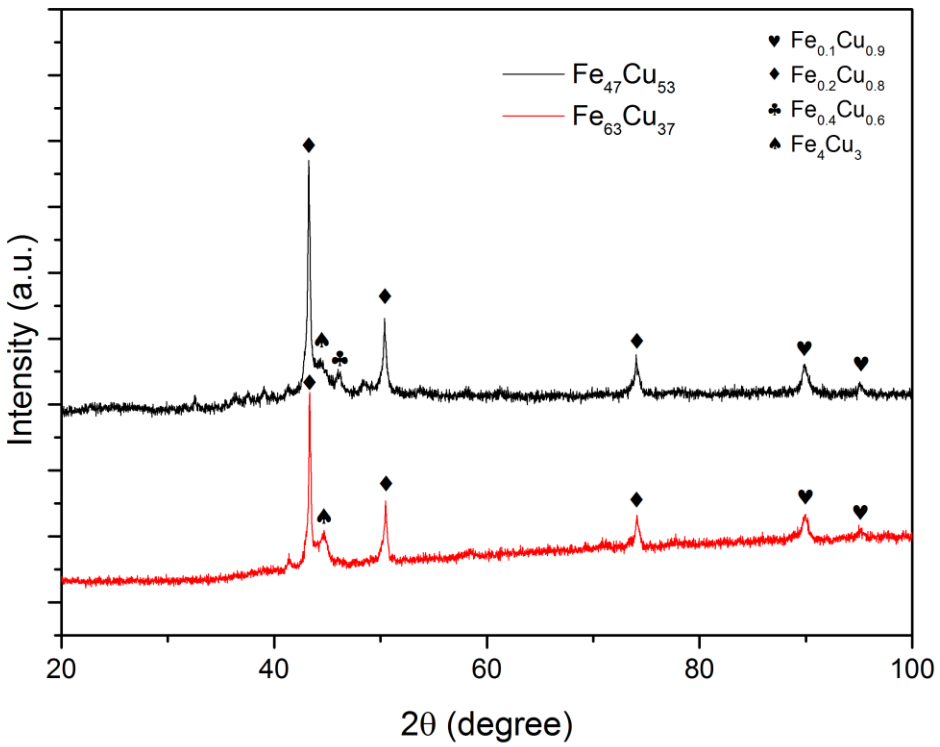

Fig. 24. XRD patterns of Fe/Cu and Fe_2/Cu (twisted wires)

4.3 Transmission and Backscattering

Fig. 25 to Fig. 28 show the delta transmission & backscattering of Fe particles, Cu particles, Fe-Cu mixed particles and Fe/Cu particles in ethanol solution, respectively. The values have been determined by enclosed air in the bottom and on the top of the cylindrical glass tube.

In contrast to Fe particles that stabilize rapidly and reach a near-steady state after 6 hours (Fig. 25), Cu particles take longer, the stabilization process is more gradual (Fig. 26). Stabilization process of Fe-Cu mixed powder (Fig. 26) and Fe/Cu powder (Fig. 27) take place at medium speed, between the two cases above, with Fe/Cu experiment slightly faster.

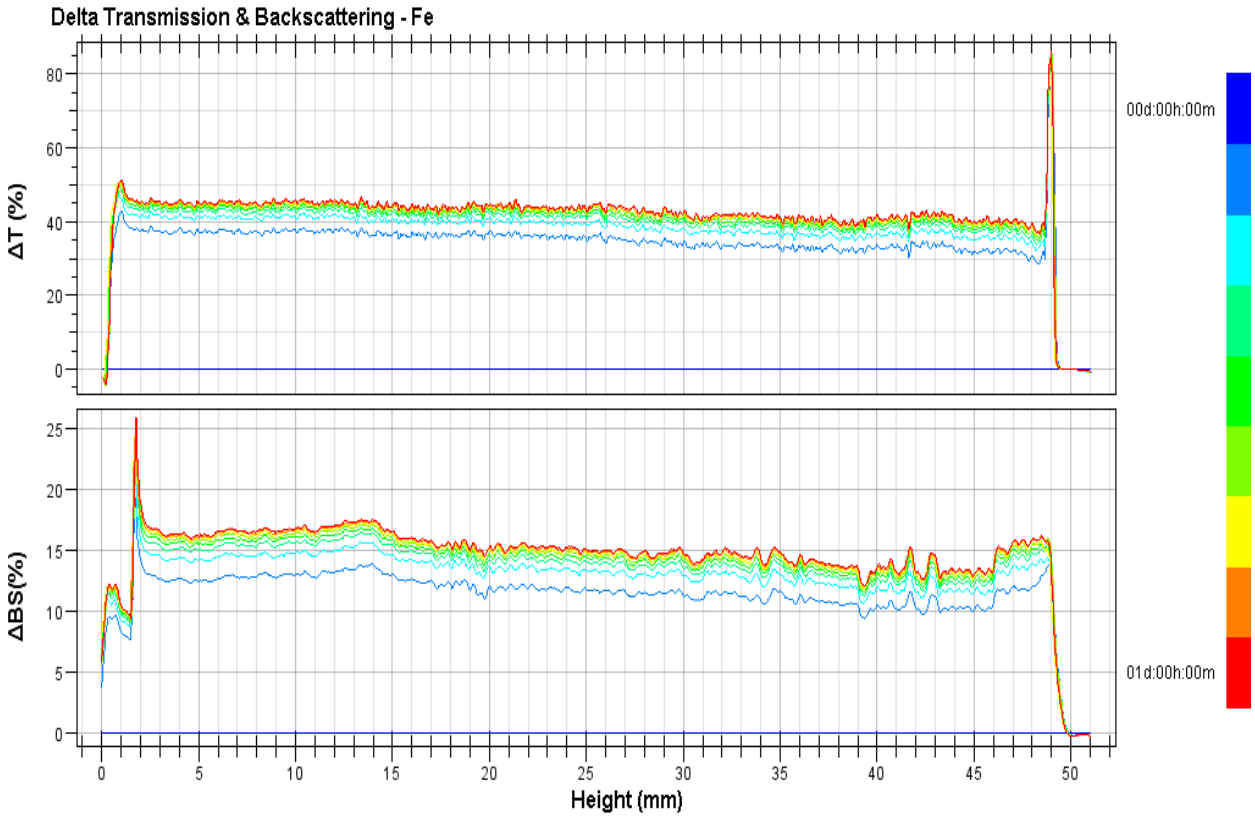

Fig. 25. Delta transmission & backscattering of Fe

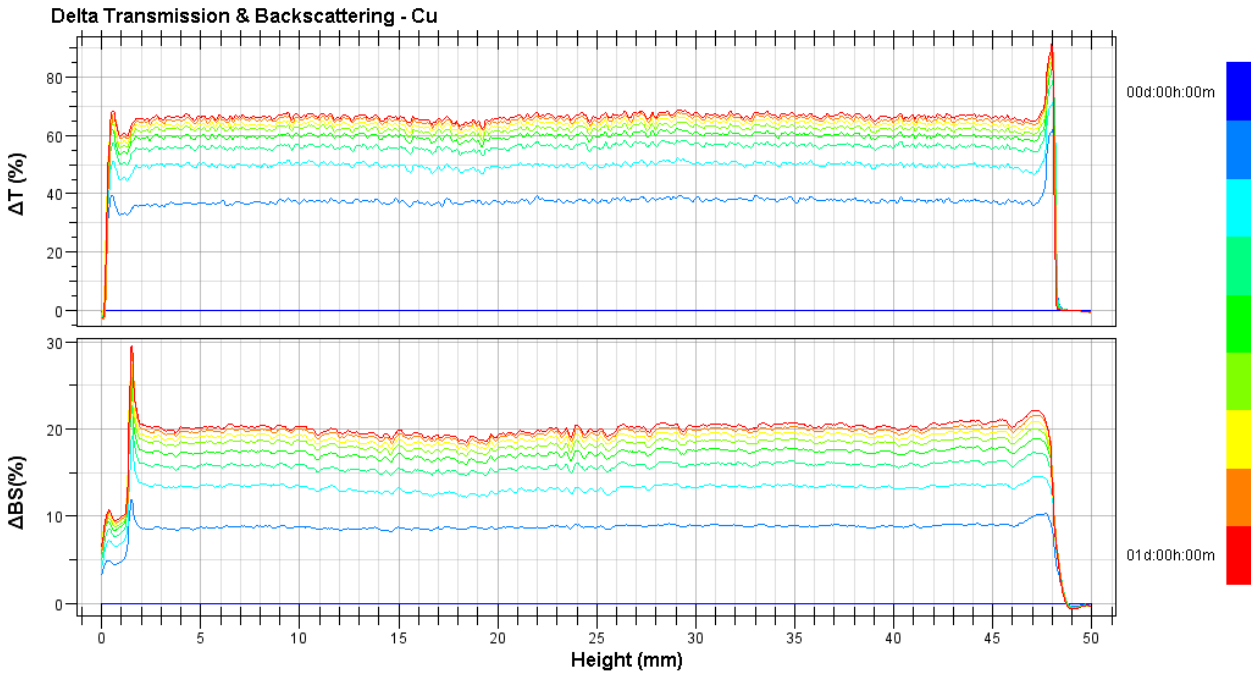

Fig. 26. Delta transmission & backscattering of Cu

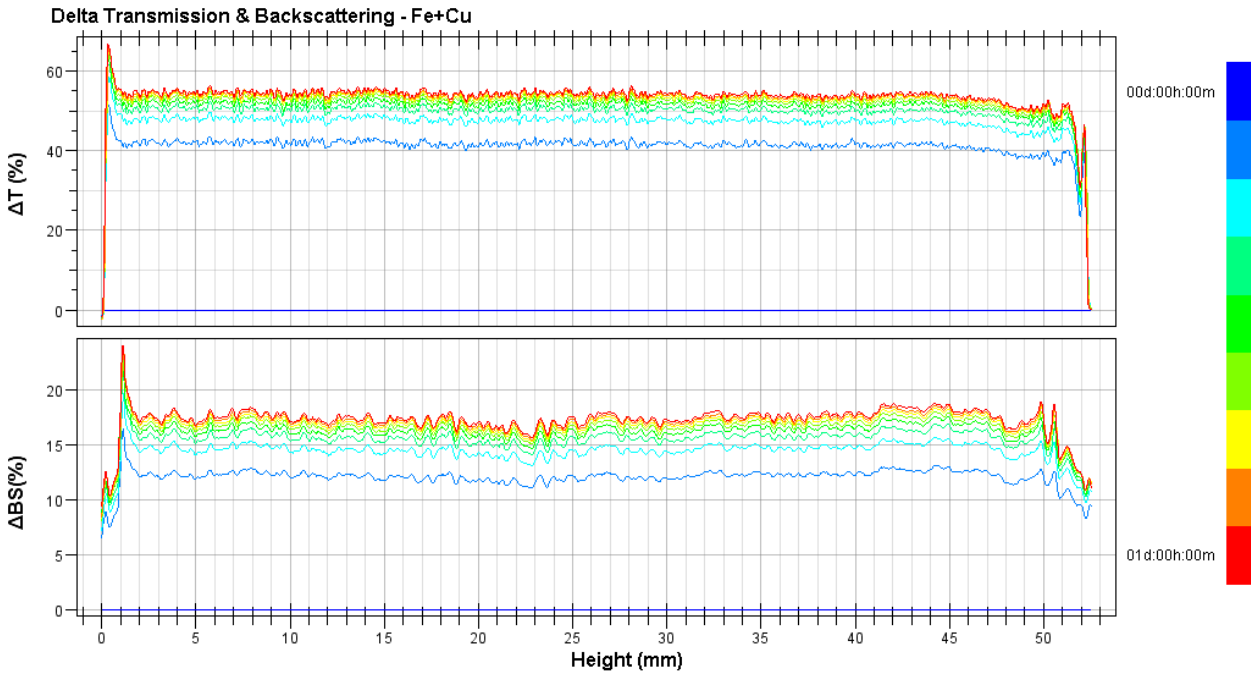

Fig. 27. Delta transmission & backscattering of Fe-Cu mixed

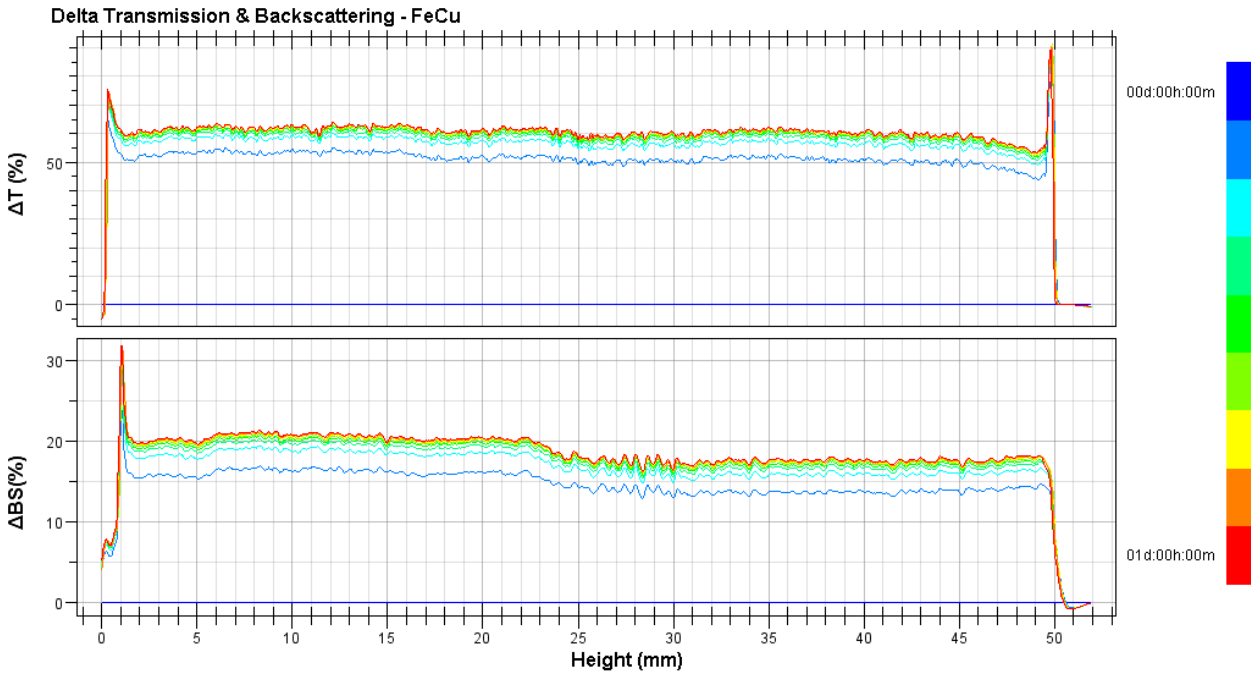

Fig. 28. Delta transmission & backscattering of Fe/Cu

Fig. 29. show the destabilisation kinetics of there four powders. As in latest result, copper powder's kinetic is the least stabilization, and copper has the highest kinetic among the powders after one day. Other powders have more stable kinetics, which increase rapidly during the first three hours and slower thereafter. The mean values of these powders can be observed at Fig. 30. Copper powder also stands out with dissimilar mean value of transmission while others have approximate values.

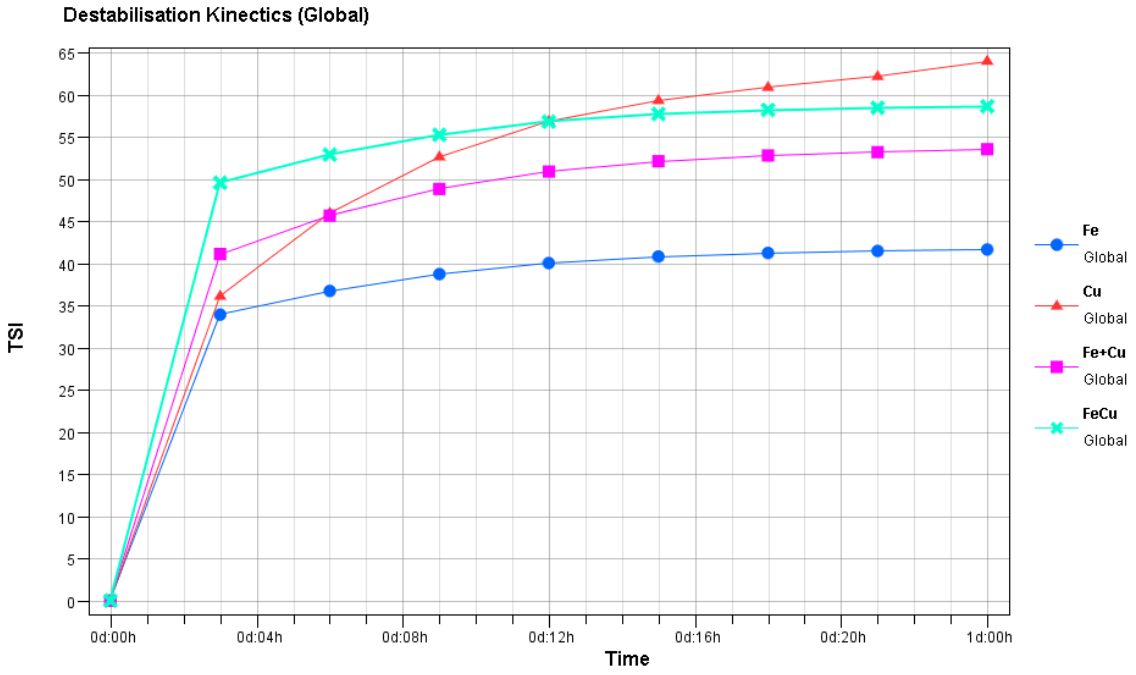

Fig. 29. Destabilisation kinetics of powders

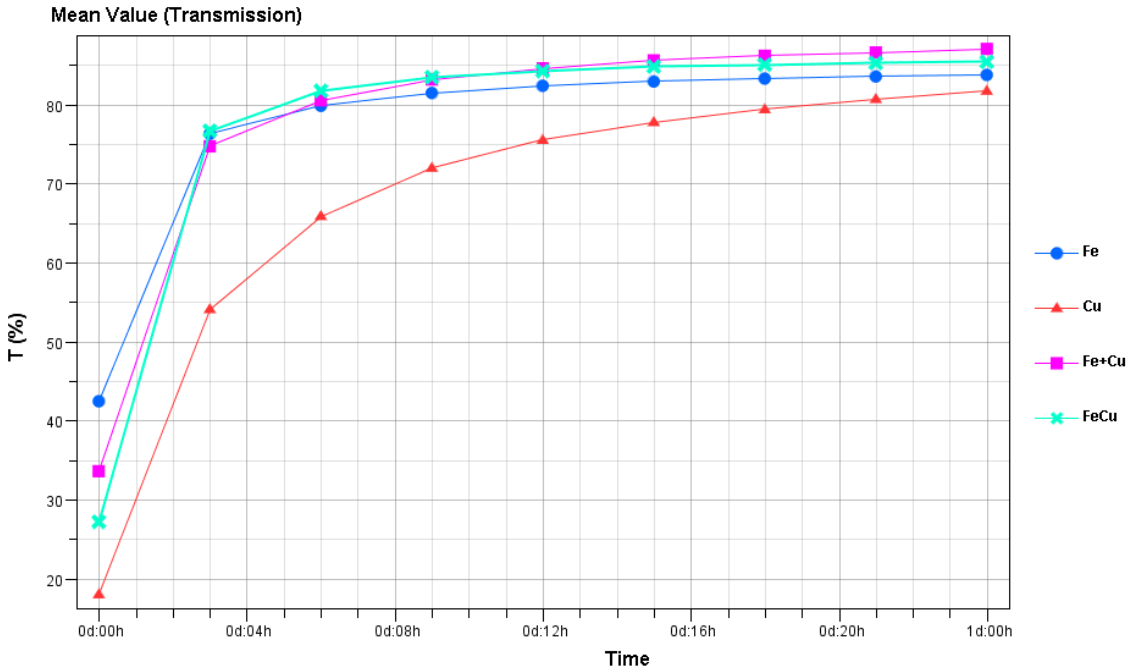

Fig. 30. Mean values of powders (transmission)

Chapter 5 - Summary and Conclusions

In summary, the present work has successfully fabricated the Fe/Cu nanopowders by using explosion of twisted wires in ethanol. Control factors were electrical parameters, characteristics of wires, and surrounding ambiences.

Despite their little mutual solubility in the solid state, the nanoparticles were prepared and their characteristics were investigated. The nanopowders were nearly spherical shape with the mean particle size distribution range from 10-200 nm, but mostly is under 100 nm. Compare among the experiments, because of the difference in the melting point and the electrical conductivity between Fe and Cu, it tends to increase the number of small particles with higher Fe content in the twisted wires. Also, TEM images show that the as-synthesized nanoparticles were covered by a very thin graphitic carbon layer due to the existence of carbon element in the ethanol.

According to the XRD analysis results, ethanol solution is better than DI water solution on limit the oxidation progress of metal. Metal wires will form metal oxide during explosion process but when twisted iron and copper together, instead of metal oxide, the fabricated nanoparticles consist of phases of $Fe_{0.1}Cu_{0.9}$, $Fe_{0.2}Cu_{0.8}$, $Fe_{0.4}Cu_{0.6}$, and Fe_4Cu_3. The alloy synthesis phases will be determined by the input composition.

This work showed a simple and promising method to synthesize the metastable Fe/Cu alloys. The obtained nano-sized particles can be a promising material to be applied widely in environmental and medical applications.

Reference

1. Boverhof, D.R., et al., *Comparative assessment of nanomaterial definitions and safety evaluation considerations.* Regulatory Toxicology and Pharmacology, 2015. **73**(1): p. 137-150.
2. Hübler, A.W. and O. Osuagwu, *Digital quantum batteries: Energy and information storage in nanovacuum tube arrays.* Complexity, 2010. **15**(5): p. 48-55.
3. McGovern, C., *Commoditization of nanomaterials.* Nanotechnology Perceptions, 2010. **6**: p. 155-178.
4. Buzea, C., I.I. Pacheco, and K. Robbie, *Nanomaterials and nanoparticles: Sources and toxicity.* Biointerphases, 2007. **2**(4): p. MR17-MR71.
5. Sharma, G., et al., *Novel development of nanoparticles to bimetallic nanoparticles and their composites: A review.* Journal of King Saud University - Science, 2019. **31**(2): p. 257-269.
6. Kessler, R., *Engineered nanoparticles in consumer products: understanding a new ingredient.* Environmental health perspectives, 2011. **119**(3): p. a120-a125.
7. Wang, Y. and Y. Xia, *Bottom-Up and Top-Down Approaches to the Synthesis of Monodispersed Spherical Colloids of Low Melting-Point Metals.* Nano Letters, 2004. **4**(10): p. 2047-2050.
8. Iravani, S., *Green synthesis of metal nanoparticles using plants.* Green Chemistry, 2011. **13**(10): p. 2638-2650.
9. Iqbal, P., J.A. Preece, and P.M. Mendes, *Nanotechnology: The "Top-Down" and "Bottom-Up" Approaches*, in *Supramolecular Chemistry*. 2012.
10. Xia, Y. and G.M. Whitesides, *Soft Lithography.* Angew Chem Int Ed Engl, 1998. **37**(5): p. 550-575.
11. Kim, H.J., K.J. Kim, and D.S. Kwak, *A Case Study on Modeling and Optimizing Photolithography Stage of Semiconductor Fabrication Process.* Quality and Reliability Engineering International, 2010. **26**(7): p. 765-774.
12. Ochekpe, N.A., P.O. Olorunfemi, and N.C. Ngwuluka, *Nanotechnology and Drug Delivery Part 2: Nanostructures for Drug Delivery.* Tropical Journal of Pharmaceutical Research, 2009. **8**(3): p. 275-287.
13. Teo, B.K. and X.H. Sun, *From top-down to bottom-up to hybrid nanotechnologies: Road to nanodevices.* Journal of Cluster Science, 2006. **17**(4): p. 529-540.
14. van Manen, H.J., et al., *Non-Covalent Chemistry on Surface-Confined, Isolated Dendrimers.* Advanced Functional Materials, 2002. **12**(1112): p. 811-818.
15. O'Dwyer, C., et al., *Bottom-up growth of fully transparent contact layers of indium tin oxide nanowires for light-emitting devices.* Nat Nanotechnol, 2009. **4**(4): p. 239-44.
16. Sondi, I. and B. Salopek-Sondi, *Silver nanoparticles as antimicrobial agent: a case study on E. coli as a model for Gram-negative bacteria.* J Colloid Interface Sci, 2004. **275**(1): p. 177-82.
17. Rai, M., A. Yadav, and A. Gade, *Silver nanoparticles as a new generation of antimicrobials.* Biotechnol Adv, 2009. **27**(1): p. 76-83.
18. Nanda, A. and M. Saravanan, *Biosynthesis of silver nanoparticles from Staphylococcus aureus and its antimicrobial activity against MRSA and MRSE.* Nanomedicine, 2009. **5**(4): p. 452-6.

19. Espinosa-Cristobal, L.F., et al., *Antibacterial effect of silver nanoparticles against Streptococcus mutans.* Materials Letters, 2009. **63**(29): p. 2603-2606.
20. Toshima, N. and T. Yonezawa, *Bimetallic nanoparticles—novel materials for chemical and physical applications.* New Journal of Chemistry, 1998. **22**(11): p. 1179-1201.
21. Stamenkovic, V.R., et al., *Improved oxygen reduction activity on Pt3Ni(111) via increased surface site availability.* Science, 2007. **315**(5811): p. 493-7.
22. Huang, X., et al., *ELECTROCHEMISTRY. High-performance transition metal-doped Pt(3)Ni octahedra for oxygen reduction reaction.* Science, 2015. **348**(6240): p. 1230-4.
23. Jia, Q., et al., *Activity descriptor identification for oxygen reduction on platinum-based bimetallic nanoparticles: in situ observation of the linear composition-strain-activity relationship.* ACS Nano, 2015. **9**(1): p. 387-400.
24. Ferrando, R., J. Jellinek, and R.L. Johnston, *Nanoalloys: from theory to applications of alloy clusters and nanoparticles.* Chem Rev, 2008. **108**(3): p. 845-910.
25. Chen, P.C., et al., *Tip-Directed Synthesis of Multimetallic Nanoparticles.* J Am Chem Soc, 2015. **137**(28): p. 9167-73.
26. Tao, F.F., *Synthesis, catalysis, surface chemistry and structure of bimetallic nanocatalysts.* Chem Soc Rev, 2012. **41**(24): p. 7977-9.
27. Sankar, M., et al., *Designing bimetallic catalysts for a green and sustainable future.* Chem Soc Rev, 2012. **41**(24): p. 8099-139.
28. Hakim, S.H., et al., *Synthesis of supported bimetallic nanoparticles with controlled size and composition distributions for active site elucidation.* Journal of Catalysis, 2015. **328**: p. 75-90.
29. Alloyeau, D., et al., *Size and shape effects on the order-disorder phase transition in CoPt nanoparticles.* Nat Mater, 2009. **8**(12): p. 940-6.
30. Sellmyer, D.J., et al., *Novel structures and physics of nanomagnets (invited).* Journal of Applied Physics, 2015. **117**(17): p. 172609.
31. Kuisma, M., et al., *Localized surface plasmon resonance in silver nanoparticles: Atomistic first-principles time-dependent density-functional theory calculations.* Physical Review B, 2015. **91**(11): p. 115431.
32. Zaleska-Medynska, A., et al., *Noble metal-based bimetallic nanoparticles: the effect of the structure on the optical, catalytic and photocatalytic properties.* Adv Colloid Interface Sci, 2016. **229**: p. 80-107.
33. Ghosh Chaudhuri, R. and S. Paria, *Core/shell nanoparticles: classes, properties, synthesis mechanisms, characterization, and applications.* Chem Rev, 2012. **112**(4): p. 2373-433.
34. AshaRani, P.V., et al., *Cytotoxicity and genotoxicity of silver nanoparticles in human cells.* ACS Nano, 2009. **3**(2): p. 279-90.
35. Parimaladevi, R., et al., *Synergistic effects of copper and nickel bimetallic nanoparticles for enhanced bacterial inhibition.* Materials Letters, 2018. **211**: p. 82-86.
36. Hasebe, M. and T. Nishizawa, *Further study on phase diagram of the iron-copper system.* Calphad, 1981. **5**(2): p. 105-108.
37. Huang, X. and T. Mashimo, *Metastable BCC and FCC alloy bulk bodies in Fe–Cu system prepared by mechanical alloying and shock compression.* Journal of Alloys and Compounds, 1999. **288**(1-2): p. 299-305.

38. Weeber, A.W., *Application of the Miedema Model to Formation Enthalpies and Crystallization Temperatures of Amorphous-Alloys.* Journal of Physics F-Metal Physics, 1987. **17**(4): p. 809-813.
39. He, J., J.Z. Zhao, and L. Ratke, *Solidification microstructure and dynamics of metastable phase transformation in undercooled liquid Cu–Fe alloys.* Acta Materialia, 2006. **54**(7): p. 1749-1757.
40. Mazzone, G. and M.V. Antisari, *Structural and magnetic properties of metastable fcc Cu-Fe alloys.* Phys Rev B Condens Matter, 1996. **54**(1): p. 441-446.
41. Bakina, O.V., et al., *«Janus»-like Cu-Fe bimetallic nanoparticles with high antibacterial activity.* Materials Letters, 2019. **242**: p. 187-190.
42. Ma, E., M. Atzmon, and F.E. Pinkerton, *Thermodynamic and magnetic properties of metastable FexCu100−xsolid solutions formed by mechanical alloying.* Journal of Applied Physics, 1993. **74**(2): p. 955-962.
43. Xu, J., et al., *Formation of supersaturated solid solutions in the immiscible Ni–Ag system by mechanical alloying.* Journal of Applied Physics, 1996. **79**(8): p. 3935-3945.
44. Yavari, A.R., P.J. Desre, and T. Benameur, *Mechanically driven alloying of immiscible elements.* Phys Rev Lett, 1992. **68**(14): p. 2235-2238.
45. Hansen, M., K. Anderko, and H.W. Salzberg, *Constitution of binary alloys.* Journal of the Electrochemical Society, 1958. **105**(12): p. 260C-261C.
46. Klement, W., *Solid solutions in copper-iron alloys quenched rapidly from the melt.* TRANS METALL SOC AIME, TRANSACTIONS, 1965. **233**(6): p. 1180-1182.
47. Kneller, E.F., *Magnetic and Structural Properties of Metastable Fe-Cu Solid Solutions.* Journal of Applied Physics, 1964. **35**(7): p. 2210-2211.
48. Chien, C.L., et al., *Magnetic properties of FexCu100-x solid solutions.* Phys Rev B Condens Matter, 1986. **33**(5): p. 3247-3250.
49. Sumiyama, K. and Y. Nakamura, *Metastable Crystalline and Amorphous Fe Alloys Produced by Vapor Quenching*, in *Rapidly Quenched Metals*, S. Steeb and H. Warlimont, Editors. 1985, Elsevier. p. 859-862.
50. Huang, L.J. and B.X. Liu, *Spontaneous vitrification in an immiscible Fe-Cu system.* Applied Physics Letters, 1990. **57**(14): p. 1401-1403.
51. Uenishi, K., et al., *Mechanical Alloying in the Fe-Cu System.* Zeitschrift Fur Metallkunde, 1992. **83**(2): p. 132-135.
52. Yavari, A.R. and P.J. Desré, *Ordering and disordering in alloys*. 1992: Elsevier. 414.
53. Bachmaier, A., et al., *The formation of supersaturated solid solutions in Fe–Cu alloys deformed by high-pressure torsion.* Acta Mater, 2012. **60**(3): p. 860-871.
54. Nastasi, M. and J.W. Mayer. *Ion Beam Mixing*. in *Radiation Effects in Solids*. 2007. Dordrecht: Springer Netherlands.
55. Nazarenko, O., *Nanopowders produced by electric explosion of wires.* 2007.
56. Kwon, Y.-S., et al., *Electroexplosive Technology of Nanopowders Production: Current Status and Future Prospects.* Journal of Korean Powder Metallurgy Istitute, 2012. **19**: p. 40-48.
57. Alsawafta, M., et al., *Kinetics at the nanoscale: formation and aqueous oxidation of copper nanoparticles.* Reaction Kinetics, Mechanisms and Catalysis, 2011. **104**(2): p. 437-450.